

A simulation study of field-induced proton-conduction pathways in dry ionomers

This article has been downloaded from IOPscience. Please scroll down to see the full text article.

2011 J. Phys.: Condens. Matter 23 234105

(<http://iopscience.iop.org/0953-8984/23/23/234105>)

View [the table of contents for this issue](#), or go to the [journal homepage](#) for more

Download details:

IP Address: 134.99.64.185

The article was downloaded on 06/10/2011 at 16:25

Please note that [terms and conditions apply](#).

A simulation study of field-induced proton-conduction pathways in dry ionomers

Elshad Allahyarov^{1,2,3}, Philip L Taylor^{1,4} and Hartmut Löwen²

¹ Department of Physics, Case Western Reserve University, Cleveland, OH 44106, USA

² Heinrich-Heine Universität Düsseldorf, Institut für Theoretische Physik II, Universitätstrasse 1, Düsseldorf 40225, Germany

³ Joint Institute for High Temperatures, Russian Academy of Sciences (IVTAN), 13/19 Izhorskaya street, Moscow 125412, Russia

E-mail: taylor@case.edu

Received 30 June 2010, in final form 16 September 2010

Published 25 May 2011

Online at stacks.iop.org/JPhysCM/23/234105

Abstract

The morphological changes that can be induced in a dry ionomer by application of a strong electric field have been studied by means of computer simulation. The internal energy of the membrane at first slowly decreases with increasing field, but then rapidly increases after a certain threshold field is reached. This effect is interpreted as the reorganization of interacting head group dipoles in response to the external perturbation. The resulting morphology contains continuous channels of hydrophilic material capable of facilitating proton conduction. Upon removal of the poling field, the system does not return to its original morphology, but retains the anisotropic structure of the poled material. The poled structure appears to be thermodynamically stable, as confirmed by calculations of the Helmholtz energy of the original and poled samples.

(Some figures in this article are in colour only in the electronic version)

1. Introduction

Perfluoro-sulfonated ionomer membranes such as Nafion are benchmark materials for proton-conducting membranes in terms of performance and stability [1–4]. These membranes are characterized by their long, hydrophobic, fluorinated, main chain and their short sidechains terminated by hydrophilic sulfonate anion groups. The chemical dissimilarity between the backbone and sidechain leads to a partially phase-segregated morphology, with comparatively sharp interfaces between the hydrophilic and hydrophobic regions. The sulfonic-acid functional groups aggregate to form a hydrophilic domain that readily absorbs water. It is within this continuous domain that ionic conductivity occurs: protons dissociate from their anionic counterion and become mobile in the presence of the hydration water. The ionic conductivities can be enhanced by an increase in concentration of the sulfonic groups, but this occurs at the expense of the mechanical strength and resistance

to excessive swelling in the presence of water molecules. A high level of hydration limits the maximum operating temperature to the vicinity of the boiling point of water. Active research is still in progress in an attempt to discover alternative ionomers with improved conductivities under low water-absorption conditions. One direction this activity can take is to find effective ways to control the connectivity of the hydrophilic regions in dry ionomers.

The network connectivity in a dry membrane strongly influences the resulting conductivity when the membrane is hydrated. The internal structure in a Nafion dispersion, and particularly the cluster-like structure created by the hydrophilic sidechain groups, pre-exists in the dry membrane. To improve the macrophase separation in wet ionomers one thus has to begin with a template having a percolation path of head groups in the dry membranes. Then, when soaked in water, this percolated network of sulfonates will produce paths along which the proton conductivity will be facilitated, even at lower water content.

⁴ Author to whom any correspondence should be addressed.

The self-assembly of dry ionomers into an inhomogeneous microstructure is mainly governed by the dipole–dipole attractions between the polar end groups of the sidechains. Beginning with a seminal paper by Eisenberg [5], a number of theoretical investigations of this microphase separation in ionomer membranes have been performed. The original Gierke model [6] suggests the existence of inverted globular micelles interconnected by a micellar channel structure. Other models propose bilayer, lamellar and sandwich-like structures for nanophase separation in membranes. Recent alternative approaches are based on more complex micelle–channel models [7–9]. For example, in [8] the Nafion membrane is described as an aggregation of polymeric chains forming elongated objects (simplified as cylinders), embedded in a continuous ionic medium. A new model of cylindrical inverted micelles is proposed in [9]. However, no consensus generally exists as to the organization of the percolating network of sulfonates in hydrated and dry ionomers.

The goal of this paper is to investigate by computer simulations the morphological changes in dry Nafion-like ionomers induced by strong applied electric fields. The motivation for our study is twofold. First, in fuel cells the ion-conducting membrane is always subjected to strong internal electric fields at the electrode contact. Second, the knowledge gained from this study can shed light on the feasibility of enhancing the formation of hydrophilic channels in ionomers by applying electric fields. We in fact show that an applied field can induce chain-like cluster formation of head groups oriented along the field direction, which is a phenomenon recently indicated by the experimental results of Lin *et al* [10]. Our numerical results indicate that membranes whose structure has been modified by strong electric fields are thermodynamically stable, and do not revert to isotropic structures when the field is removed.

Our work was partly inspired by the recent experimental advances in preparing heterogeneous ion-exchange membranes reported by Lin *et al* [10] and Oren *et al* [11] and by the improved electrodes for fuel cells reported by Middleman [12] and Wang *et al* [13]. In [11] it was found that the application of an alternating electric field during curing of the polymeric matrix resulted in the agglomeration of the ionic groups in long chains extending across the membrane. As a result, the percolation threshold for ion conduction was reduced to about 25% of its value for membranes with randomly distributed particles. In [12, 13] it was shown that the poling of Nafion at the membrane–electrode interface above T_g can lead to the alignment of carbon-black particles perpendicular to the membrane surface.

The simulations reported here build on our previous studies of hydrated membranes [14, 15]. While one may simulate the application of strong electric fields to hydrated ionomers by artificially suppressing the electrolytic decomposition of water, actual poling experiments at high fields are limited to the dry material. It is thus useful to attempt to understand fully the response of the ionomer in the absence of water of hydration.

The rest of this paper is organized as follows. In section 2 we discuss the nature of electrostatic interactions in dry

Nafion-like membranes while in section 3 we describe the simulation model and the system parameters we use for our ionomeric membrane. Section 4 is devoted to an analysis of the results so obtained, and we conclude in section 5.

2. Electrostatic interactions in dry ionomers

Nafion-like ionomers have many properties in common with diblock copolymers, amphiphiles and charged polymers. For diblock copolymers and amphiphiles, the morphology is largely determined by the short-range interaction between their constituents. The morphology of ionomers, however, is most strongly influenced by the long-range electrostatic interactions between charged species. Thus, when applying a coarse-graining approach to ionomers it is necessary to keep intact the dipolar nature of head groups.

For simplicity, we consider a simple model for a Nafion-like ionomer in which the head group dipole consists of a sulfonate ion SO_3^- to which is attached a proton H^+ . The screening length in this system, according to Jonscher [16], is

$$R_s = l \exp(\lambda_D^2/l^2). \quad (1)$$

Here $\lambda_D = (4\pi n\lambda_B)^{-1/2}$ is the Debye screening length in the charged system of SO_3^- and H^+ ions, $\lambda_B = e^2/\epsilon k_B T$ is the Bjerrum length, e is a positive elementary charge, ϵ is the dielectric permittivity of the medium, k_B is Boltzmann's constant, T is the absolute temperature, n is the concentration of charged particles, and l is the length of the dipole created by the sulfonate group SO_3^- and its attached proton H^+ . The resulting SO_3H dipoles have zero net charge and thus experience no net force as a response to external fields. We do not concern ourselves with the behavior of a single dipole inside the cluster of dipoles, nor the distribution of the ions and dipoles within ionic clusters, as an extensive study of these effects and the effects of the rotation of individual dipoles within a given cluster in response to dipole–dipole interactions, mechanical stiffness of the pendant chain and external loading are given in [17, 18].

3. Simulation model and system parameters

We implement a united-atom model for the Nafion-like ionomer membrane, in an approach similar to that used in our previous papers [15, 19, 20] and elsewhere [21–23]. Within the coarse-grained model, the fluorocarbon CF_2 groups of the backbone, and the CF_2 and CF_3 groups, the sulfur atom, the oxygen O_3 group, and the attached proton of the sidechains are modeled as Lennard-Jones (LJ) monomers of a diameter $\sigma = 0.35$ nm. The backbone polymer is considered to be completely electroneutral. The structural model for Nafion in our simulations is schematically illustrated in figure 1. For sidechains we consider two different charge distributions for monomers. Within the simple charge distribution (SCD) model, only the terminal group monomers are charged. We write $q_S = +1.1e$, $q_{\text{O}_3} = -2.1e$ and $q_H = +1e$. For the partial charge distribution (PCD) model for the sidechains, all the sidechain monomers carry the nonzero partial charges adopted

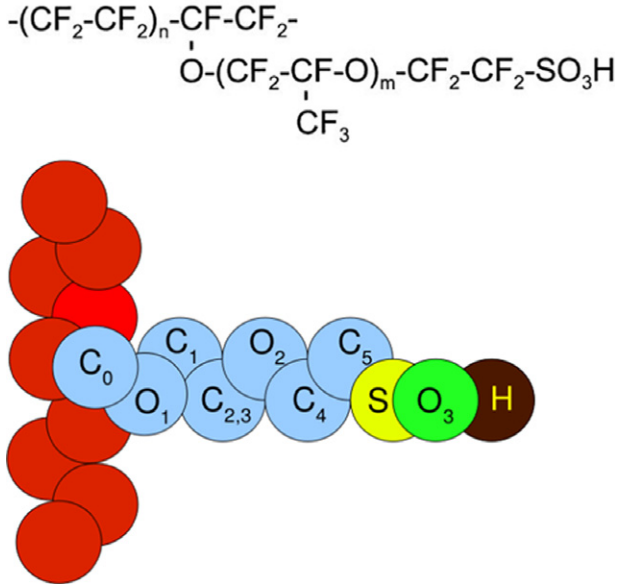


Figure 1. Top line: Nafion structure. Lower illustration: the coarse-grained model used in this work. Light gray (blue online) spheres and spheres with inscribed atom labels represent the sidechain. Dark gray (red online) spheres form the backbone segment of the polymer. The head group units are explicitly assigned in this illustration.

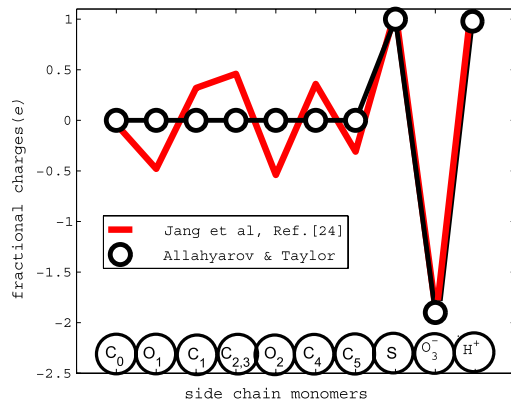


Figure 2. Sidechain charge distribution in the SCD model (line with circles) and the PCD model (solid line, from the work of Jang *et al* [24]).

from [24]. In the PCD model the head group monomers are charged as: $q_S = +1.08e$, $q_{O_3} = -1.85e$ and $q_H = +1e$. Thus the terminal group SO_3H , in contrast to the SCD model, has a small positive charge $+0.23e$, which is compensated for by the negative charge on the rest of the sidechain. The sidechain charge distributions in the SCD and PCD models are illustrated in figure 2, and are listed in table 1.

The total potential energy of the membrane is

$$\begin{aligned}
 U(\vec{r}) = & \sum_i U_b(b_i) + \sum_j U_\theta(\theta_j) + \sum_m U_\varphi(\varphi_m) \\
 & + \sum_{k,l} U_{nb}(|\vec{r}_k - \vec{r}_l|),
 \end{aligned} \quad (2)$$

where $\vec{r} = (\vec{r}_1, \vec{r}_2, \dots, \vec{r}_N)$ is the set of three-dimensional position vectors of the N membrane monomers. In equation (2)

Table 1. Sidechain PCDs in the SCD and PCD models. The designation in the first column corresponds to the monomer labels in figure 1. The first monomer C_0 is a common monomer for the sidechain and the backbone segments.

Sidechain monomers	SCD charges	PCD charges
C_0	0	-0.04
O_1	0	-0.48
C_1	0	0.32
$C_{2,3}$	0	0.46
O_2	0	-0.54
C_4	0	0.36
C_5	0	-0.31
S^+	+1.1	+1.08
O_3^-	-2.1	-1.85
H^+	+1	+1

the index i runs over all chain bonds, j runs over all bond angles, m runs over all torsional angles, and k and l run over all non-bonded pairs in the system. The non-bonded interaction term in equation (2) is a combination of electrostatic Coulomb interactions between each pair of charged particles and the 6-12 LJ potential between monomers. The LJ interaction parameters and corresponding force-field coefficients in equation (2) were chosen to be the same as in [20].

Molecular dynamic simulations were performed for a dry membrane at a constant volume $V = (11 \text{ nm})^3$ and a constant temperature $T = 300 \text{ K}$. There were 14 backbone monomers between adjacent sidechains. The molar concentration, η , of sulfonates in the simulation box was 2 mol l^{-1} . The system temperature was controlled by a Langevin thermostat with a friction coefficient $\gamma = 2 \text{ ps}^{-1}$ and a Gaussian noise of strength of $6k_B T \gamma$. The equations of motion were integrated using the velocity Verlet algorithm with a time step of 0.5 fs. Standard periodic boundary conditions with Lekner summation of long-range electrostatic interactions [25] were imposed. To avoid having chain entanglements interfere with equilibration, we adopted the procedure of occasionally cutting the polymer into fragments, partially equilibrating, and then reassembling the polymer for further equilibration as described in [15, 20, 26–28]. We expect this process to result in a membrane conformation that progresses rapidly to a minimum internal free energy, as the otherwise insurmountable entanglement barriers can then be obviated.

4. Simulation results

4.1. Internal energy

Dry Nafion, having been equilibrated during simulation runs lasting 10 ns, was subjected to a constant, uniform electric field E oriented parallel to the z -axis of the simulation box, and equilibrated for a further 3–5 ns. This external field generates an electric force $\vec{F}_z = q_i \vec{E}$ that acts on all charged ions i in the sidechains. The total number of charges N_i in the simulated system depends on the sidechain model implemented, SCD or PCD.

In figure 3 the internal energy U of the membrane, defined as the membrane potential energy without the membrane–field interaction term, is plotted as a function of applied field E .

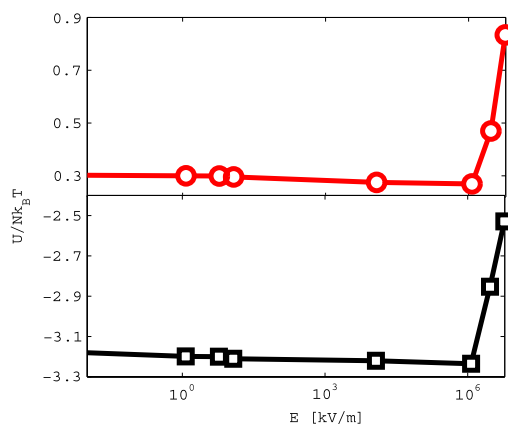


Figure 3. A nonlinear response of the internal potential energy U of the membrane to the applied field E . Bottom line with squares—PCD model, upper line with circles—SCD model.

The internal energy at first gently decreases as the strength E of the field is increased, until, beyond a threshold value $E_0 \approx 10^6 \text{ kV m}^{-1}$, the internal energy increases rapidly. This phenomenon takes place for both the SCD and PCD sidechain architectures.

We attribute this sharp increase in internal energy to the breaking of the dipole–dipole pairing that occurs in the dry material. In the absence of a strong applied field, the

head groups tend to cluster in such a way that the sulfonate units are grouped in adjacent pairs in which the dipoles are oppositely oriented. This lowers the Coulomb energy of interaction between them, and the equilibrium state of the membrane then consists of material that is isotropic on the macroscopic scale, but in which the structure is heterogeneous on the nanometer scale. The hydrophilic clusters contain randomly oriented groupings of sulfonates, as can be seen in figure 4(a), and these are at first little affected by the applied field. The small decrease in internal energy results from the change in the energy landscape that permits small sulfonate groupings to move intact to positions of lower energy. It is only when the field becomes sufficiently strong to break the oppositely ordered pairing of the dipoles that an anisotropic chain-like ordering of the dipoles occurs. The internal energy then increases rapidly, while the (negative) energy of interaction with the applied field increases even more rapidly. We note that the sign of U in figure 3 differs in the PCD and SCD models. The negative U in the PCD model stems from the Coulomb interactions taken into account in the last term of equation (2). When the membrane has fully charged sidechains, as in the PCD model, the sidechain conformation changes to take advantage of its most favorable orientation.

When the external field is removed, and the system is again equilibrated, the field-induced anisotropy does not

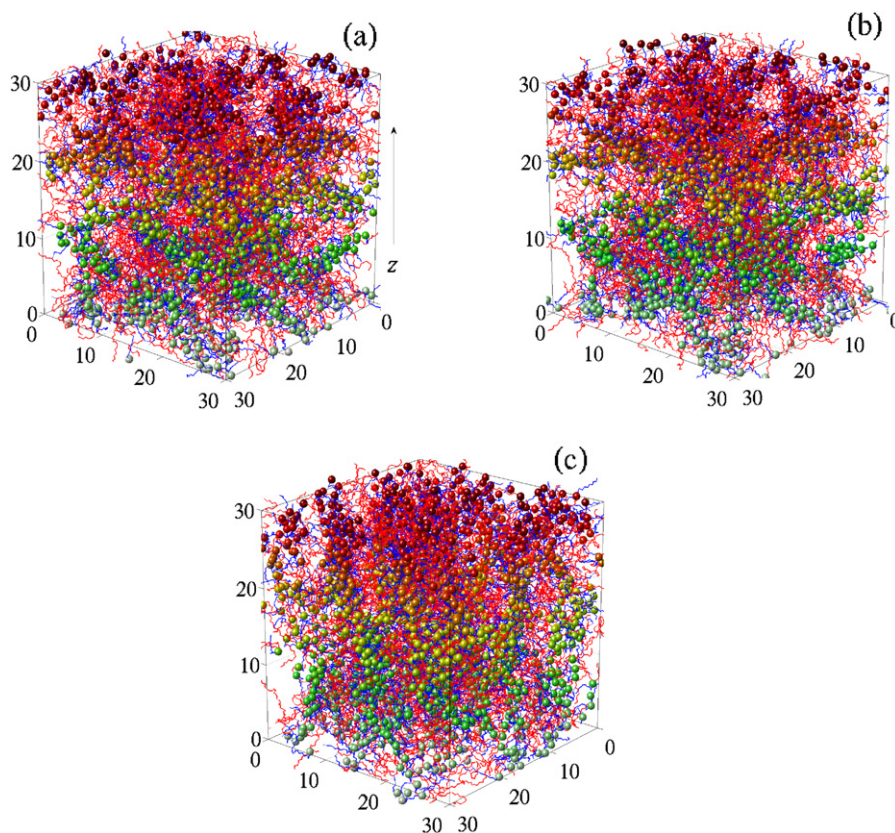


Figure 4. Snapshot pictures from simulation boxes for differently treated membranes with the SCD charges for sidechains. The spheres represent the end group oxygen atoms of sidechains. The pendant sidechain and neutral backbone chains are drawn by lines (in blue and red correspondingly online). To aid perspective, spheres at the top of the simulation box are shown darker (red online) and those at the bottom are shown lighter (green online). The size of all structural elements is schematic rather than space filling. (a) Untreated membrane A, (b) weakly poled membrane B, (c) strongly poled membrane C.

Table 2. Configurational parts of the internal energy $U/(Nk_B T)$ from equation (2) and the excess Helmholtz free energies $\Delta A/(Nk_B T)$ for the untreated membrane *A*, and for the poled membranes *B* and *C*. The subscripts 1 and 2 refer to the SCD and PCD models for sidechain charges. N is the total number of membrane monomers in the simulation box.

Membrane	A_1	B_1	C_1	A_2	B_2	C_2
$U/(Nk_B T)$	0.30	0.16	0.13	-3.20	-3.22	-3.31
$\Delta A/(Nk_B T)$	-6.19	-6.22	-6.27	-9.47	-9.50	-9.54

disappear, as can be seen in the simulation snapshots portrayed in figure 4. Figure 4(a) shows the initial sample before the poling field has been applied, and shows no macroscopic anisotropy. We refer to this as membrane *A*. Figure 4(b) shows the same material after the application and then removal of a poling field of strength $E = 10^6$ kV m⁻¹. We refer to this as membrane *B*, while membrane *C* has been poled with a field of $E = 8 \times 10^6$ kV m⁻¹. The thread-like structure of sulfonates that persists after the field is removed, and which can serve as a pathway for a proton diffusion when the membrane is hydrated, is mostly clearly visible in membrane *C*. The question of whether these states are thermodynamically stable is addressed in section 4.3.

In order to distinguish the different membrane morphologies belonging to different electric field treatments, we refer to the membranes as A_n , B_n or C_n , where the index $n = 1$ ($n = 2$) stands for the SCD (PCD) model. The total energies $U/Nk_B T$ of these membranes, according to equation (2), are given in table 2. It is evident that the pretreated states have potential energies smaller than the initial membrane. In other words, the applied field helps the membrane to overcome energy barriers and access a new and energetically favorable state.

4.2. Structural analyses of poled membranes

In section 4.1 we noted the reduction in energy resulting from the poling treatment of membranes. In this section we probe the morphologies of the membranes *A*, *B* and *C* using standard approaches such as the calculation of sulfonate–sulfonate pair correlation functions $g_{ss}(r)$ and the corresponding structure factors $S_{ss}(k)$ for sidechain sulfonates, and the structure factors $S_{bb}(k)$ for the backbone monomers. The curves $g_{ss}(r)$ for the SCD and PCD models are plotted in figure 5. Being a spherically averaged quantity, $g_{ss}(r)$ is not capable of distinguishing between the states *A* and *B*. The correlation curves for the membranes *A* and *B* look similar regardless of the fact that the state *B* has an internal energy smaller than the state *A*. This tendency is visible for both the sidechain charge distributions SCD and PCD, shown correspondingly in figures 5(a) and (b). A single peak at $r = 1.35\sigma$ corresponds to the smallest sulfur–sulfur distances in sulfonate clusters. The membrane *C* has longer-scale correlations, represented by the peaks beyond the primary multiplet peak. These cluster peaks correspond to the elongation of clusters along the applied field. The simulation result for a version of the strongly poled membrane *C* having a reduced concentration of sulfonates is shown in figure 5(a) as a dashed line. At smaller sulfonate–sulfonate separations the correlation curves in figure 5 for

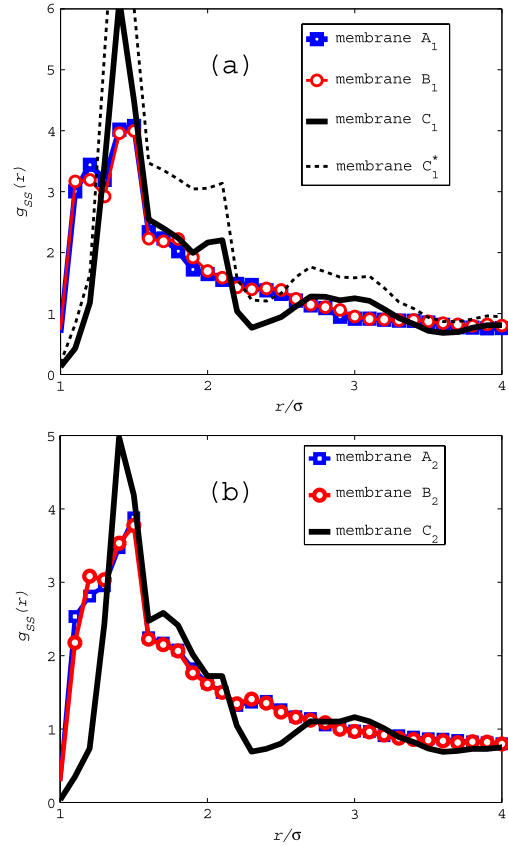


Figure 5. Sulfonate–sulfonate pair correlation functions $g_{ss}(r)$ for membrane states *A*, *B* and *C*. (a) The SCD sidechain model and (b) the PCD sidechain model. The dashed line in (a) is for a reduced sulfonate concentration $\eta = 1.4$ mol l⁻¹. The other examples have $\eta = 2.0$ mol l⁻¹.

membranes *A* and *B* are above the curve for the membrane *C*. This is a clear indication of the distortion of multiplets induced by a strong external field. We note that the uneven charge distribution along the sidechain in the PCD model tends to decrease the association of head groups. This is evident, for example, from the comparison of the curves for the state *C* in figure 5. It thus seems that, for an effective nanophase separation and clustering of head groups, it is better to design sidechains with charges mostly located on their head groups.

Whereas the pair correlations $g_{ss}(r)$ reveal the short-range morphology of sulfonate clusters, the study of structure factors is a more convenient approach for probing the system morphologies at nano-size distances. We calculate the structure factors directly in simulations using the relation

$$S_l(k) = \frac{1}{N_l} \left\langle \sum_{r_i} \sum_{r_j} \exp(i\vec{k} \cdot \vec{r}_{ij}) \right\rangle. \quad (3)$$

Here N_l is the number of particles of type l in the simulation box, $l = s, b$, respectively, for sulfonates and backbone monomers, \vec{k} is a wavelength vector with Cartesian components $k = 2\pi n_p/L$, $n_p = \pm 1, \pm 2, \dots$, $\vec{r}_{ij} = \vec{r}_i - \vec{r}_j$. The extent of phase segregation in the system is usually deduced from the low-wavenumber peak of $S_{ss}(k)$, shown in figure 6(a). For the untreated initial membrane *A* there are

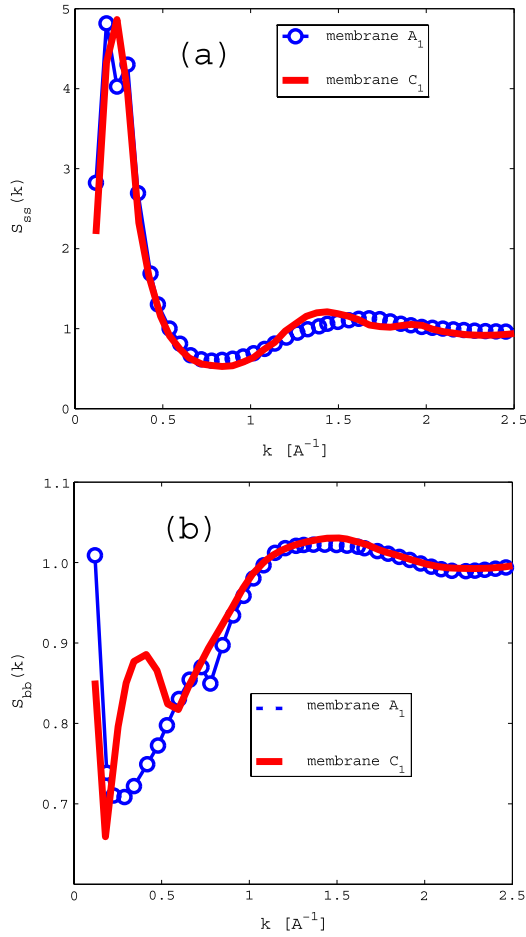


Figure 6. (a) Sulfonate–sulfonate structure factor $S_{ss}(k)$ and (b) backbone–backbone structure factor $S_{bb}(k)$ for the SCD sidechain model. The results for the PCD model, not shown, are qualitatively similar.

two peaks at positions $k = 0.18$ and 0.30 \AA^{-1} . In real space these positions correspond to the density correlations at the length scales of 35 and 21 \AA . Both these values are in good agreement with the ionomer peak position observed in scattering experiments [24, 29, 30]. For the poled membrane C, there is a single peak at $k = 0.24 \text{ \AA}^{-1}$, which is 26 \AA in real space. The final network of ordered sulfonates, after the field is removed, thus resembles a network of connected clusters of size around 26 \AA .

Structure factors calculated for the backbone are shown in figure 6(b). Here membrane C exhibits backbone ordering, corresponding to the peak position at $k = 0.42 \text{ \AA}^{-1}$, which does not appear in the membranes A and B. This ordering has a length scale of 15 \AA , roughly half of the cluster size for sulfonates. We speculate that the field-induced ordering in the sulfonate system facilitates a corresponding cluster formation in the ionomer backbone. Unfortunately we are not able to probe the formation of larger backbone crystallites because of the size limits of our simulation box, which makes the minimum accessible wavevector k equal to $2\pi/L$. The experimentally reported values $k = 0.01\text{--}0.05 \text{ \AA}^{-1}$ [2],

attributed to the size of backbone crystalline domains, are below the value $k_{\min} = 0.11 \text{ \AA}^{-1}$ accessible in our simulations. However, it seems likely that domains of size 15 \AA are the building blocks for larger crystallites in the backbone.

4.3. Free energy and channel-forming analyses

In this subsection we analyze the stability of states A, B and C. A relevant thermodynamic potential for the NVT ensemble is the Helmholtz free energy $\mathcal{A} = E - TS$. Here E is the internal energy (the sum of the potential and kinetic energies of membrane components) and S is the system entropy. While the calculation of E is straightforward, the calculation of the entropy for charged membranes is a challenging task. A method based on the acceptance ratios of Boltzmann distributions during a single molecular dynamics simulation was developed by Hong *et al* [31] and successfully applied to water, to hard-dumbbell fluids [32], and to hard-sphere and LJ fluids [33]. However, our test simulations using this method showed this approach to be inefficient when applied to systems with large-scale density correlations. We therefore used a classical thermodynamic integration (TI) method to calculate the relative free energies of membranes A, B and C. In this approach, we first calculate the difference $\Delta\mathcal{A}$ between the free energy reached in a simulation of membrane A and the free energy of the same system when all the strong Coulomb interactions are removed. We repeat this procedure for membranes B and C. If the removal of Coulomb interactions turns out to lead to apparently the same unstructured material in all three cases, then we have a comparison of the free energies of the three membranes when Coulomb interactions are present.

We accordingly form

$$\Delta\mathcal{A}/(Nk_B T) = 1/(Nk_B T) \int_{\xi=0}^{\xi=1} \langle \partial H(\xi)/\partial \xi \rangle d\xi. \quad (4)$$

Here the coupling parameter ξ characterizes the strength of Coulomb interactions U_c^{ij} between charges i and j , so that $U(\xi) = \xi U_c^{ij}$. The configurational part of the parametrized Hamiltonian $H(\xi)$ is chosen as $U_{\text{conf}}(\xi) = U + (\xi - 1) \sum_{i>j} U_c^{ij}$, where the first term U is the total potential energy of a chosen state. The integrand $\langle \partial H(\xi)/\partial \xi \rangle$, which reduces to $\langle U(\xi) \rangle$, is a smooth function of the parameter ξ , and is plotted in figure 7. Our simulations show that, when $\xi = 0$, the case of a totally neutral membrane, all three membrane states, A, B and C, have indistinguishable morphologies with equal correlation functions and internal potential energies. The calculated excess free energies per membrane monomer $\Delta\mathcal{A}_i/(Nk_B T)$, $i = A, B, C$, are given in table 2. In fact, it is the difference $\Delta\mathcal{A}_{ij} = \Delta\mathcal{A}_i - \Delta\mathcal{A}_j$, that determines which membrane is thermodynamically stable. For the SCD sidechain model the free energy differences are $\Delta\mathcal{A}_{BA}/(Nk_B T) = -0.03$, $\Delta\mathcal{A}_{CA}/(Nk_B T) = -0.08$. Thus, compared to the initial membrane A, the poled membranes B and C are thermodynamically favored, with membrane C being the most stable. A similar tendency is observed for the PCD model as well: $\Delta\mathcal{A}_{BA}/(Nk_B T) = -0.03$, $\Delta\mathcal{A}_{CA}/(Nk_B T) = -0.04$. We note that the free energy differences here are given

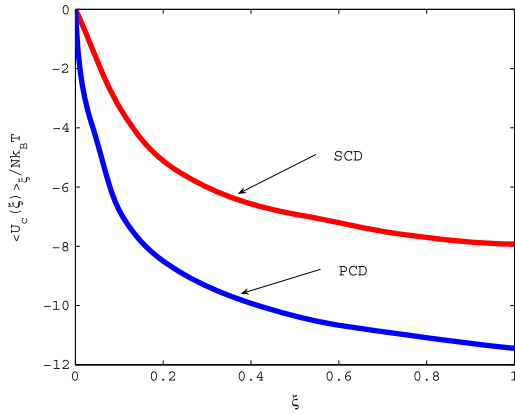


Figure 7. The integrand of equation (4) as a function of the strength parameter ξ of the Coulomb interaction between ionomer charges for membrane *C* with the SCD and PCD charges for sidechains.

per membrane monomer. When recalculated per sulfonate the free energy differences will be 24 times larger. Thus, given that an ordinary cluster in ionomer structures comprises at least 30–50 sulfonates, the free energy difference between an elongated cluster in poled membrane and a shapeless cluster in untreated membrane will be in the range 40–80 $k_B T$. This corresponds to an energetic barrier which can be crossed only by ionomer molding.

We have thus confirmed that the external field helps the membrane to overcome the potential energy barriers that stand in the way of achieving a more stable conformation. The fact that extremely strong fields are required is an indication of the height of these barriers, and suggests that elevated temperatures may be needed to accompany poling by more modest fields if the same goal is to be achieved, namely the ordering of the sulfonates into a structure morphologically similar to the ordering we find in membrane *C*.

The correlation functions $g_{ss}(r)$ and $S_{ss}(k)$, discussed in section 4.2, are not helpful in the examination of the bridging between sulfonate clusters. Because such bridging is crucial to enable proton diffusion along the continuous pathways in fuel cell membranes, we require a procedure to identify the distribution of lengths Λ of continuous hydrophilic pathways within the ionomer. The details of the method we use are given in the appendix. We define a continuous pathway as connecting sulfonates that are no further apart than a maximum separation distance r_{\max} . Distribution functions $P(\Lambda)$ for $r_{\max} = 6 \text{ \AA}$, which is the average separation between the sulfonates in the head group channels according to the calculated correlation functions in figure 5, are shown in figure 8 for the SCD and PCD models. The long-range behavior of $P(\Lambda)$ is seen to depend strongly on the membrane’s history. In the strongly poled membrane *C*, the hydrophilic channels are about 50% longer than in the more weakly poled membrane *B*, and are twice as long as in the unpoled membrane *A*. It is also seen from figure 8(b) that the PCD charges of the sidechains hinder channel formation in membrane *C*. In other words, the smaller the charges on the hydrophobic part of the sidechain, the longer are the pathways formed when the material is poled.

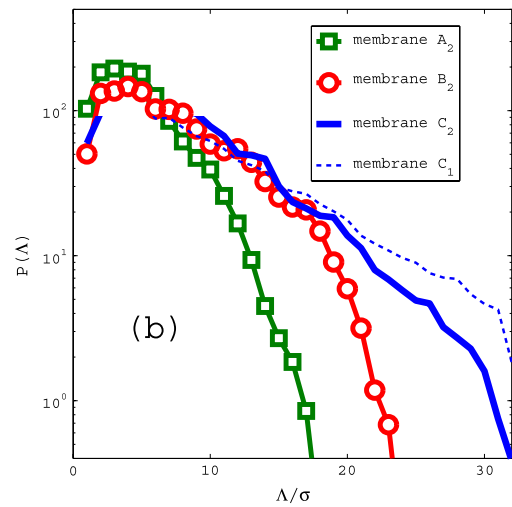
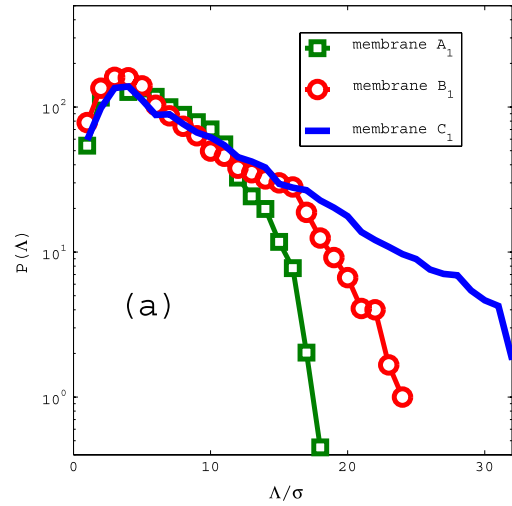


Figure 8. The probability distribution $P(\Lambda)$ for finding a continuous pathway of sulfonate SO_3^- ions of length Λ for different sidechain charge representations. (a) SCD model and (b) PCD model.

Because our simulation box size was only 31.4σ , the channels found in membrane *C* are effectively infinite. The corresponding three-dimensional sulfonate density for membrane *C*, shown in figure 9, gives a visual confirmation of the formation of continuous pathways for proton conduction.

5. Conclusion

We have investigated the morphological changes produced in a dry ionomer by the action of applied electric fields. In an ionomer prepared by equilibration from an arbitrary starting point, there is a balance between the attractive electrostatic forces between head group dipoles and the elastic forces within the polymer backbone. The resulting equilibrated state of the membrane contains an internal tension associated with the mechanical resistance from the backbone material to the structural relaxation of the sidechains. This prevents the sidechains from forming the chain-like structures that might

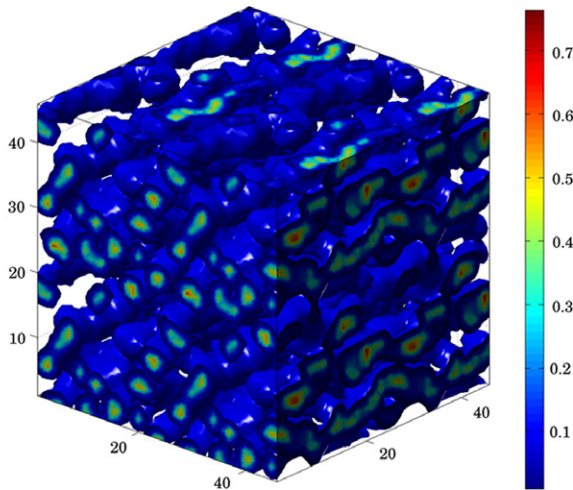


Figure 9. Sulfonate density distribution for the strongly poled membrane *C* within the SCD sidechain model.

minimize the Coulomb energy. Exposing the membrane to a strong external electric field subjects its head groups to forces sufficient to cause chain formation. This induced ordering in the sidechain terminal groups is a desirable morphology for conducting membranes, since it has a lower percolation threshold at low hydration. The proximity of sulfonate head groups in these channels facilitates proton hopping between adjacent sulfurs at low wetting conditions [34].

The lowering of internal stress in the polymer backbone can be also achieved through increasing the ionic mobility by adding excess water. This method, used in the solvent-casting of membranes, does not, however, lead to the formation of aligned states of sulfonates. This is a consequence of the fact that in dissolved ionomers, electrostatic interactions between negatively charged sulfonates, positively charged free ions and dipolar water molecules lead to a short-range effective attraction between sulfonates. As a result of this attraction the sulfonates cluster into globular micelle-like aggregates. Upon the evaporation of water, the membrane shrinks in size and the micelles approach each other. The existence of a hydrophobic backbone shell around each cluster, however, obstructs the fusion of neighboring clusters into a single elongated aggregate.

One of the unexpected findings reported in this work is the existence of a ‘field-exposure’ memory in the membrane. The morphological changes induced by external fields are found to be irreversible, and this can be accounted for by their apparently lower Helmholtz energy.

We also note that the poling structures in dry ionomers discussed here are different from the structures formed in poled low-water membranes. In [14, 15] it was found that, when there are from one to five water molecules per sulfonate, the field-generated current of protons facilitates the formation of rod-like sulfonate clusters with hexatic order perpendicular to the applied field. This structure remained stable with a lower equilibrium energy in the remnant membrane after the removal of poling. However, recent poling simulations of high-water membranes, in which there are more than eight water

molecules per sulfonate group, revealed that the remnant rod-like structure is energetically unstable. Cylindrical clusters first disaggregate into separate parts, which then form a 3D percolated network with no memory of the structural ordering from previous poling.

The uneven charge distribution along the sidechain in the PCD model is found to decrease the association of head groups into clusters, and hinders the formation of long proton pathways in the field-exposed membrane. The strongly poled membrane also exhibits a backbone ordering that is not present in untreated or weakly poled membranes.

In conclusion, the simulations reported here suggest a means for improving hydrophilic channeling in ionomers by the use of strong poling electrostatic fields. While it was necessary to apply very high fields in simulations lasting only a few nanoseconds, we expect that a similar effect could be achieved by the application of more modest fields for much longer times, and at elevated temperatures.

Acknowledgments

This work was supported by the US Department of Energy under Grant DE-FG02-05ER46244, and was made possible by the use of facilities at the Case ITS High Performance Computing Cluster and the Ohio Supercomputing Center.

Appendix. Procedure to measure the proton pathway length

The procedure used is illustrated schematically in figure A.1 and consists of the following steps.

- (i) A sulfonate unit i is randomly chosen, and its neighbors inside a sphere of radius r_{\max} (the unbroken circle in the figure A.1) are identified.
- (ii) For each of these neighbors j , a new sphere is drawn (broken circle in the figure), and a list of its neighbors k is compiled.

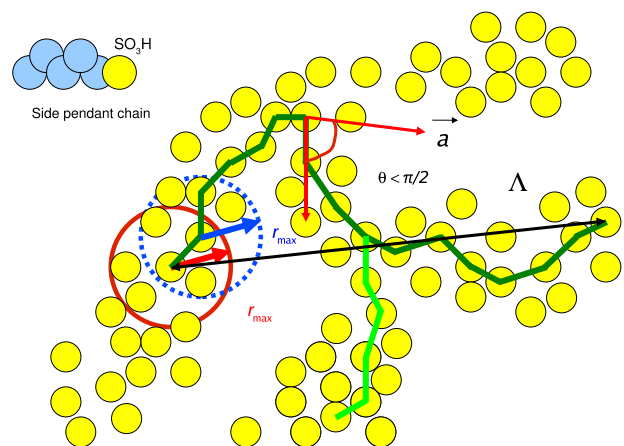


Figure A.1. Illustration of the procedure described in the appendix for finding the length distribution of continuous pathways linking hydrophilic groups. The spheres represent the head groups, and the dark line marks a pathway of length Λ .

- (iii) In order to reduce the likelihood of closed loops being traced, we delete from the list those neighbors for which the angle θ between the two consecutive path vectors \vec{a}_{ij} and \vec{a}_{jk} is greater than $\pi/2$.
- (iv) The procedure is repeated until the maximum path length Λ_{\max} is found or until Λ exceeds the size of the simulation box.
- (v) The distribution $P(\Lambda)$ of hydrophilic channel lengths Λ is then formed.

References

- [1] Gierke T D et al 1981 *J. Polym. Sci. Phys. Edn* **19** 1687
- [2] Mauritz K A and Moore R B 2004 *Chem. Rev.* **104** 4535
- [3] Kreuer K D et al 2004 *Chem. Rev.* **104** 4637
- [4] de Bruijn F 2005 *Green Chem.* **7** 132
- [5] Eisenberg A 1970 *Macromolecules* **3** 147
- [6] Hsu W Y and Gierke T D 1982 *Macromolecules* **15** 101
Hsu W Y and Gierke T D 1982 *J. Membr. Sci.* **13** 307
- [7] Ioselevich A S et al 2004 *J. Phys. Chem. B* **108** 11953
- [8] Gebel G and Diat O 2005 *Fuel Cells* **5** 261
Rubatat L et al 2004 *Macromolecules* **37** 7772
- [9] Schmidt-Rohr K and Chen Q 2008 *Nature Mater.* **7** 75
- [10] Lin H L et al 2006 *J. Polym. Res.* **13** 379
- [11] Oren Y et al 2004 *J. Membr. Sci.* **239** 17
- [12] Middelmann E 2002 *Fuel Cell Bull.* **11** 9
- [13] Wang Z T et al 2008 *J. Power Sources* **186** 293
- [14] Allahyarov E and Taylor P 2009 *Phys. Rev. E* **80** 020801
- [15] Allahyarov E and Taylor P 2009 *Phys. Rev. E* **81** 031805
- [16] Jonscher A K 2001 *IEEE Trans. Dielectr. Electr. Insul.* **8** 345
- [17] Weiland L M and Leo D J 2005 *J. Appl. Phys.* **97** 13541
- [18] Weiland L M and Leo D J 2004 *Smart Mater. Struct.* **13** 323
- [19] Allahyarov E and Taylor P 2007 *J. Chem. Phys.* **127** 154901
- [20] Allahyarov E and Taylor P 2009 *J. Phys. Chem. B* **113** 610
- [21] Wescott J T et al 2006 *J. Chem. Phys.* **124** 134702
- [22] Vishnyakov A and Neimark A V 2001 *J. Phys. Chem. B* **105** 7830
Vishnyakov A and Neimark A V 2001 *J. Phys. Chem. B* **105** 9586
- [23] Yamamoto S et al 2004 *14th Int. Conf. on the Properties of Water and Steam (Kyoto)* p 411
- [24] Jang S S 2004 *J. Phys. Chem. B* **108** 3149
- [25] Mazars M 2001 *J. Chem. Phys.* **115** 2955
- [26] Vishnyakov A and Neimark A V 2000 *J. Phys. Chem. B* **104** 4471
- [27] Rivin D et al 2004 *J. Phys. Chem. B* **108** 8900
- [28] Glotzer S C and Paul W 2002 *Annu. Rev. Mater. Res.* **32** 401
- [29] Young S K et al 2002 *J. Polym. Sci. B* **40** 387
- [30] Young S K and Mauritz K A 2001 *J. Polym. Sci. B* **39** 1282
- [31] Hong S D and Jhon M S 1997 *Chem. Phys. Lett.* **273** 79
- [32] Hong S D and Jang D J 2002 *Chem. Lett.* **31** 946
- [33] Hong S D et al 2005 *Bull. Korean Chem. Soc.* **26** 1673
- [34] Choi P et al 2005 *J. Electrochem. Soc.* **152** E123